Journal of Molecular Graphics and Modelling 37 (2012) 49–58

Contents lists available at SciVerse ScienceDirect

Journal of Molecular Graphics and Modelling

journal homepage: www.elsevier.com/locate/JMGM

Molecular basis of the initial platelet adhesion in arterial thrombosis: Molecular dynamics simulations

Jian Li, Lin Zhang, Yan Sun*

Department of Biochemical Engineering and Key Laboratory of Systems Bioengineering of the Ministry of Education, School of Chemical Engineering and Technology, Tianjin University, Tianjin 300072, China

ARTICLE INFO

Article history:
Received 2 November 2011
Received in revised form 17 March 2012
Accepted 5 April 2012
Available online 13 April 2012

Keywords:
VWF A1 domain
GPIbα
Electrostatic interactions
Hydrophobic interactions
Binding free energy

ABSTRACT

Molecular interactions between the von Willebrand factor (VWF) A1 domain and glycoprotein Ibα (GPIbα) promote the initial adhesion of platelets and subsequent arterial thrombus formation. However, little is understood about the interactions at a molecular level. Therefore, the binding dynamics and involved molecular interactions between VWF A1 domain and GPIbα in both water and physiological saline are investigated using molecular dynamics simulations and all-atom models. Faster binding is observed in water than that in physiological saline, and patches of opposite charges are observed at the binding interface. Moreover, molecular mechanics-Poisson–Boltzmann surface area analysis indicates that the binding is promoted by the long-range electrostatic interactions and then maintained by hydrophobic interactions. For the initial binding, the hot spots include the residues E14, E128, D175, D83, E151, D106, D63, E5, D18, E225, D235 in GPIbα, and K608, K569, K644, R571, K572, R636, K599 in VWF A1 domain. For the final complex formation, however, 72% of the favorable contributions are from hydrophobic interactions. The results provided molecular insight into the initial platelet adhesion. The hot spots identified would be beneficial for developing novel drugs for thrombotic diseases.

1. Introduction

Thrombosis [1–4] is associated with many arterial diseases of high mortalities [2,5], such as stroke and acute myocardial infarction. It is an exigent demand for exploring available therapeutic strategies for arterial thrombosis. Unfortunately, arterial thrombosis is a complicated process regulated by many factors [1], such as the bloodstream [6]. The microscopic information about arterial thrombosis is far from adequate. Therefore, it is necessary to investigate the microscopic process of arterial thrombosis and involved molecular interactions.

At sites of vascular injury, the formation of a hemostatic plug is necessary for normal hemostasis. However, pathologic thrombus formation can lead to thrombotic diseases. Pathologic arterial thrombosis is considered to have three important stages, including initial adhesion, firm adhesion and platelet aggregation. The von Willebrand factor (VWF) is a key bridge between the platelet and collagen to mediate the initial adhesion. VWF is a protein in plasma or subendothelial cell matrix [2]. It can bind to the collagen, as well as the platelet [7–9] through the platelet surface receptor glycoprotein Ibα (GPIbα) [10,11]. The formation of sandwich complex, collagen-VWF–GPIbα promotes the initial platelet adhesion. Once the vessel wall is disrupted under pathological conditions, such as atherosclerotic plaques rupture [6,10,11], collagens will be exposed to the bloodstream [1]. Platelets then adhere to the sites of vascular injury through collagen-bound VWF [12–15]. This step causes an initial adhesion, followed by a firm adhesion and aggregation of blood platelets [2,8,16–19]. It can be seen that the interactions between VWF A1 domain and GPIbα are essential for arterial thrombosis [20–23].

For a long time, research efforts have been devoted on the arterial thrombosis and therapeutics [24], for example, experiments *in vivo* to establish animal models [25], experiments *in vitro* to investigate the platelet adhesion and aggregation [26–31]. However, little is understood about the mechanisms of arterial thrombosis, and it is difficult for current experimental approaches to explore the details at a molecular level. MD simulation [32,33] is a powerful tool which can offer clear microscopic information, and is useful to investigate the pathogenesis of disease with many successful applications [34–42]. Therefore, all-atom models and molecular dynamics (MD) simulations are used in the present study to investigate the molecular interactions between VWF A1 domain and GPIbα. Different solution conditions are considered, including water and physiological saline. The microscopic process and involved molecular interactions are examined to provide fundamental insights into arterial thrombosis, especially for the initial adhesion.

* Corresponding author. Tel.: +86 22 27409481; fax: +86 22 27406590.
E-mail addresses: linzhang@tju.edu.cn (L. Zhang), ysun@tju.edu.cn (Y. Sun).

1093-3263/$ – see front matter © 2012 Elsevier Inc. All rights reserved.
http://dx.doi.org/10.1016/j.jmgm.2012.04.002

2. Models and methods

2.1. Model construction

The all-atom model of the complex of the wide-type VWF A1 domain and GPIbα is constructed based on X-ray crystal structure at 2.6 angstrom resolution from Protein Data Bank (PDB ID: 1SQ0, http://www.rcsb.org/pdb/) [43]. In order to get the models of separated VWF A1 domain and GPIbα, the coordinates of all the atoms of GPIbα in complex are translated by 1 nm in both y and z directions. The simple point charge (SPC) model is used for water molecule. Na^+ and Cl^- are considered as charged beads. Physiological saline is NaCl solution with a mass concentration of 0.9 g/100 mL.

Three simulation systems are constructed using these models, including complex (combined VWF A1 domain and GPIbα) in physiological saline (denoted as Com_0.9), separated VWF A1 domain and GPIbα in aqueous solution (denoted as Sep_0) and physiological saline (denoted as Sep_0.9). In Com_0.9, the complex is solvated in a 10 nm × 10 nm × 10 nm cubic box containing 30,638 water molecules, 87 Na^+ and 86 Cl^- (one more Na^+ is added to neutralize the system). In Sep_0, separated VWF A1 domain and GPIbα are solvated in an 11nm × 11nm × 11 nm cubic box containing 41,643 water molecules. 1 Na^+ is added to neutralize the system. In Sep_0.9, separated proteins are solvated in an 11nm × 11nm × 11 nm cubic box containing 41,411 water molecules, 117 Na^+ and 116 Cl^-.

2.2. MD simulation

MD simulations in the NVT ensemble are performed using Gromacs 4.0.5 package (http://www.gromacs.org/) [44,45] with the Gromos96 43a1 force field [46]. The temperature is controlled at 310.15 K by the velocity-rescale (v-rescale) method with a time constant of 0.1 ps. The Verlet algorithm is used with an integration time step of 2 fs. The Linear Constraint Solver (LINCS) algorithm is applied to constrain all bonds. The Particle-mesh Ewald (PME) algorithm is used to deal with the electrostatic interactions. The cutoffs of neighbor atom list, Coulomb potential, and Lennard-Jones (LJ) potential energies are all set to 0.9 nm. The initial velocities of particles are generated according to a Maxwell distribution at 310.15 K. Then, an energy minimization is performed, followed by 20 ns MD simulation.

2.3. Conformational analysis

The minimum distance between VWF A1 domain and GPIbα (denoted as d_{min}) is calculated using g_mindist program in Gromacs, while the distance between the centers of mass (denoted as d_{com}) is calculated using g_dist. These two parameters are used to describe the binding/dissociation between VWF A1 domain and GPIbα.

In order to describe the protein conformational transition, the secondary structure is determined using the Define Secondary Structure of Proteins (DSSP) method and do_dssp program in Gromacs. The structures of VWF A1 domain and GPIbα are shown in snapshots. Furthermore, two parameters are calculated to provide the quantitative evaluation of the protein conformation: the root mean square deviation (RMSD) and the radius of gyration (R_g) [44,45]. RMSD, represents the structural changes of a protein at time t with respect to a reference structure (herein the initial structure is used), is defined as

$$\mathrm{RMSD}(t) = \left[\frac{1}{M}\sum_{i=1}^{N} m_i \left\|\mathbf{r}_i(t) - {}_i(0)\right\|^2\right]^{1/2} \quad (1)$$

where t is the time instant, N is the number of atoms, m_i is the mass of atom i, M is the mass of all the atoms, $\mathbf{r_i}(0)$ and $\mathbf{r}_i(t)$ are the positions of atom i at time 0 and t. RMSD values are calculated using g_rms program in Gromacs. R_g, represents the compactness of the protein conformation, is defined as

$$R_g = \left(\frac{\sum_i \left\|\mathbf{r}_i\right\|^2 m_i}{\sum_i m_i}\right)^{1/2} \quad (2)$$

where m_i is the mass of atom i, and $\mathbf{r}_i$ is the position of atom i with respect to the center of mass of the molecule. R_g values are calculated using g_gyrate program in Gromacs.

The snapshots are prepared using Visual Molecular Dynamics (VMD, http://www.ks.uiuc.edu/Research/vmd/). The Adaptive Poisson–Boltzmann Solver (APBS) electrostatics analysis module of VMD is used to calculate the electrostatic surface potentials of VWF A1 domain, GPIbα, and their complex.

2.4. Molecular interactions analysis

The molecular interactions between VWF A1 domain and GPIbα are described using van der Waals and electrostatic interactions. In the present study, the LJ potential energy (denoted as E_{LJ}) is used to represent short-range van der Waals interactions and to evaluate the hydrophobic interactions [47], while the Coulomb potential energy (denoted as E_C) is used to describe the electrostatic interactions. Both of them are calculated using g_energy program in Gromacs. These two parameters are defined as

$$V_{LJ}\left(r_{ij}\right) = \left(\frac{C_{ij}^{(12)}}{r_{ij}^{12}} - \frac{C_{ij}^{(6)}}{r_{ij}^{6}}\right) \quad (3)$$

$$V_C\left(r_{ij}\right) = f\left(\frac{q_i q_j}{\varepsilon_r r_{ij}}\right) \quad (4)$$

where $V_{LJ}(r_{ij})$ is the LJ potential energy between two atoms i and j, $V_C(r_{ij})$ is the Coulomb potential energy between two charged particles i and j, r_{ij} is the distance between i and j, the $C_{ij}^{(12)}$ and $C_{ij}^{(6)}$ are parameters depending on a pair of atom types, q_i and q_j represent the charge numbers, ε_r is the relative dielectric constant, f is the electric conversion factor, and $f = 1/(4\pi\varepsilon_0) = 138.935485$ kJ nm/mol/e^2.

2.5. MM–PBSA analysis

The binding free energy of VWF A1 domain–GPIbα complex is calculated using molecular mechanics-Poisson–Boltzmann surface area (MM–PBSA) method [48] and the CHARMM program (http://www.charmm-gui.org/). Herein, it should be noted that the CHARMM27 and GROMOS 43A1 force fields are used consecutively. The binding free energy is calculated based on the structures provided by the MD simulation using GROMOS 43A1 force field. As reported by Todorova et al. [49], both CHARMM27 and GROMOS 43A1 force fields provide similar structural trends of chain B of insulin. Moreover, two MD simulations on the complex have been performed for 2 ns using the same initial structure of protein but different force field. One uses the GROMOS force field and the other uses CHARMM force field. Little deviation is observed in these two simulation trajectories (data not shown). Therefore, in the present study, the CHARMM program is used to analyze the structures and the free energy decomposition is used to provide the relative evaluation of each residue.

$$\Delta G_{bind} = \Delta G_{gas} + \Delta G_{desolv} - T\Delta S \quad (5)$$

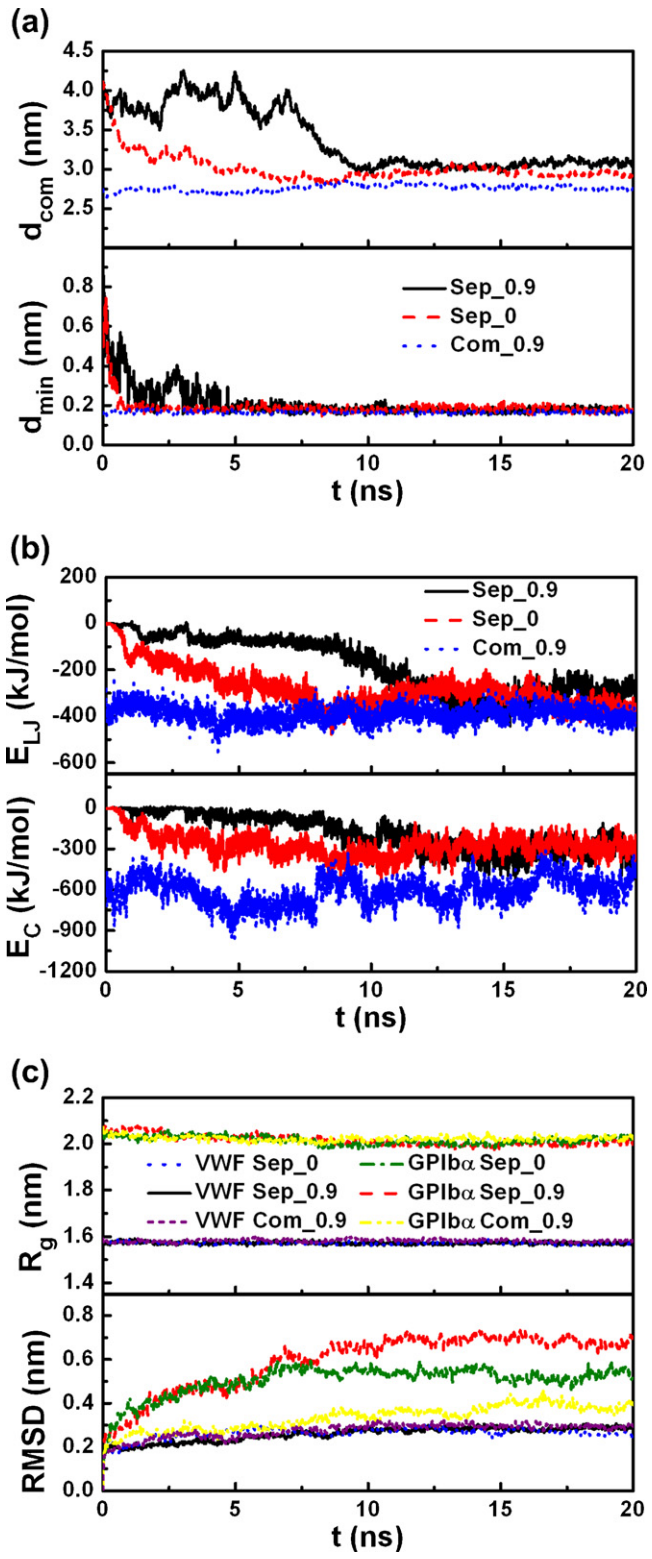

Fig. 1. Binding dynamics of the VWF A1 domain and GPIbα in water and physiological saline. (a) The time courses of d_{min} and d_{com} between VWF A1 domain and GPIbα. (b) The Coulomb and LJ potential energies between VWF A1 domain and GPIbα. (c) The RMSD and R_g values of VWF A1 domain and GPIbα. Sep_0 and Sep_0.9 represent the simulation systems of separated proteins in aqueous solution and physiological saline, respectively. Com_0.9 represents the simulation system of the complex in physiological saline.

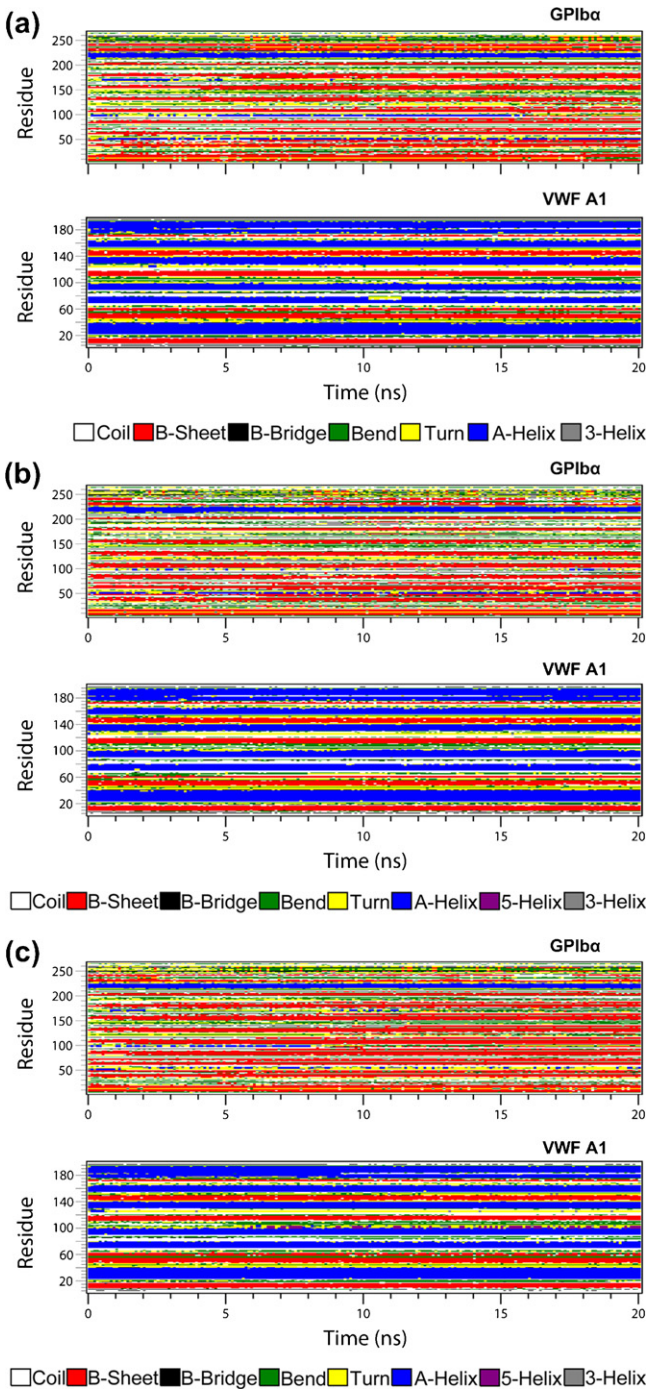

Fig. 2. Secondary structure evolution of the proteins during the dynamics processes. (a) The complex in physiological saline. (b) The proteins during the binding process in water. (c) The proteins during the binding process in physiological saline. The α-helix and β-sheet are marked in blue and red, respectively.

where ΔG_{bind} is the absolute binding free energy, ΔG_{gas} is the gas-phase contribution, ΔG_{desolv} is the desolvation energy of the system upon binding, $-T\Delta S$ is the entropic contribution. Herein, T is the temperature, and ΔS is equal to the difference between the entropy of the complex and those of the isolated proteins. In the present study, the relative free energy is analyzed without consideration of $-T\Delta S$. Moreover, the analysis concerns primarily per-residue electrostatic and hydrophobic contributions rather than the absolute binding free energy.

$$\Delta G_{gas} = \Delta G_{elec} + \Delta G_{vdW} + \Delta G_{inter} \quad (6)$$

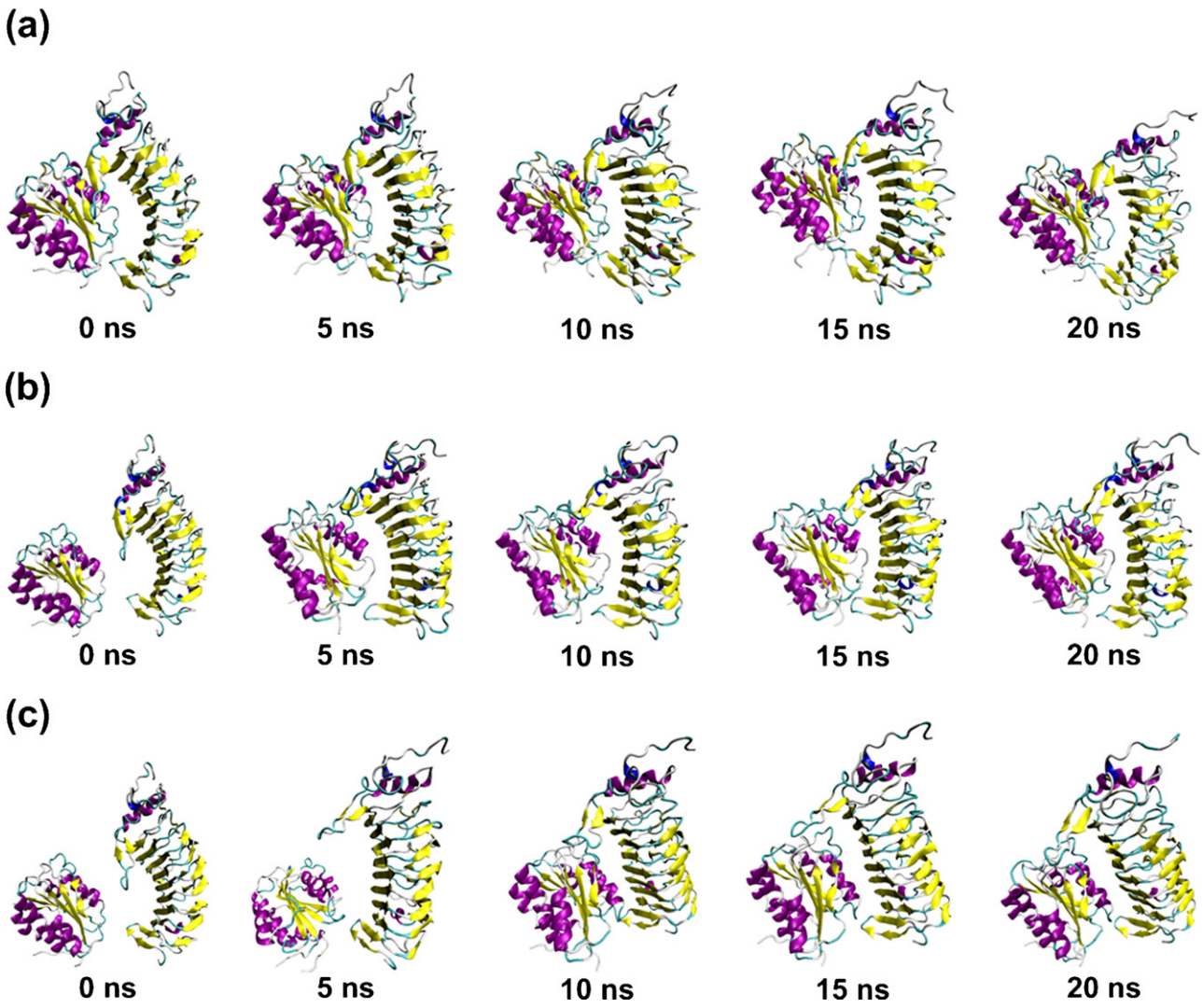

Fig. 3. Typical snapshots of the VWF A1 domain and GPIbα at different time points during the dynamics processes. (a) The complex in physiological saline. (b) The proteins during the binding process in water. (c) The proteins during the binding process in physiological saline. Globular protein on the left is VWF A1 domain, while elongated and curved protein on the right is GPIbα. Snapshots are prepared by VMD.

where ΔG_{elec} and ΔG_{vdW} are the free energies contributed by the electrostatic interactions and the van der Waals interactions between proteins, respectively. ΔG_{inter} is equal to the difference between the internal energy of the complex and those of the isolated proteins. Herein, because "the same trajectory method" [50] is used, ΔG_{inter} is equal to zero.

$$\Delta G_{desolv} = \Delta G_{PB} + \Delta G_{SASA} \tag{7}$$

$$G_{SASA} = \gamma \times SASA + b \tag{8}$$

where ΔG_{desolv} is equal to the difference between the solvation free energy of the complex and those of the isolated proteins. The solvation free energy is divided into the electrostatic and nonpolar contributions, so ΔG_{desolv} is divided into the electrostatic (ΔG_{PB}) and nonpolar (ΔG_{SASA}) terms. ΔG_{PB} is calculated by solving the linear Poisson–Boltzmann equation using the PBEQ module of the CHARMM program. The dielectric constants of the protein and aqueous environment are set to 1 and 80, respectively. The salt concentration of physiological saline is set to 0.15 mol/L (0.9 g/100 mL). The nonpolar solvation energy G_{SASA}, which can be considered as the sum of a solvent–solvent cavity term and a solute–solvent vdW term, is calculated by Eq. 8, where the constant γ is 0.00542 kcal/mol/Å^2, and b is 0.92 kcal/mol. The solvent-accessible surface area (SASA) is calculated using a water probe radius of 1.4 Å. In this way,

$$\Delta G_{bind} = \Delta G_{polar} + \Delta G_{nonpolar} \tag{9}$$

$$\Delta G_{polar} = \Delta G_{elec} + \Delta G_{PB} \tag{10}$$

$$\Delta G_{nonpolar} = \Delta G_{vdW} + \Delta G_{SASA} \tag{11}$$

where the total binding free energy ΔG_{bind}, is divided into the polar (ΔG_{polar}) and nonpolar ($\Delta G_{nonpolar}$) terms. ΔG_{polar} and $\Delta G_{nonpolar}$ are used to describe the electrostatic and hydrophobic contributions, respectively. Moreover, the binding free energy is decomposed on each residue to estimate per-residue contribution. The linear PB equation allows the decomposition of electrostatic solvation energy, since the electrostatic potential at point i, Φ_i can be calculated as the sum of the potentials created by other individual charges.

$$\Delta G^{j}_{polar} = \sum_{i \in Complex} \frac{1}{2} q_i \phi_i^{j \in Complex} - \left[\sum_{i \in VWF} \frac{1}{2} q_i \phi_i^{j \in VWF} + \sum_{i \in GPIb\alpha} \frac{1}{2} q_i \phi_i^{j \in GPIb\alpha} \right] \tag{12}$$

Half of the van der Waals term between pairwise residues is attributed to each residue in the interaction pair. The nonpolar solvation energy term of each residue is proportional to the loss in SASA of each residue.

3. Results and discussion

3.1. Molecular behavior of the complex in physiological saline

The molecular behavior of VWF A1 domain–GPIbα complex is examined in physiological saline by 20 ns molecular dynamics simulation (simulation trajectory of Com_0.9). Protein conformational transition and involved molecular interactions in the dynamic process are examined, as shown in Fig. 1 to Fig. 3.

During the simulation, the minimum distance between two proteins is almost a constant at 0.17 nm (Fig. 1a), while the distance between the centers of mass has a slight fluctuation between 2.6 and 2.9 nm, indicating stable complex. Larger Coulomb potential energy than LJ potential energy is observed (Fig. 1b), indicating strong electrostatic interactions in the complex. The fluctuations of potential energies are observed as a result of thermal motion. The Coulomb potential has large fluctuations during the simulation. The conformational transition is further examined using RMSD and R_g. Smaller RMSD of VWF A1 domain than that of GPIbα is always observed during the simulation (Fig. 1c), indicating more stable structure of VWF A1 domain. Meanwhile, the largest RMSD is 0.46 nm, which is very small in consideration of the large molecule size. In addition, R_g only has slight fluctuations, indicating minor conformational transition and stable complex.

The secondary structure evolution of proteins during the dynamics process is determined by DSSP, as shown in Fig. 2a. It can be seen that α-helix and β-sheet are the major secondary structures in VWF A1 domain and GPIbα, respectively. No significant change of secondary structure is observed during the simulation, which is consistent with the results in Fig. 1. The typical snapshots are provided in Fig. 3a for further verification. It can be seen that VWF A1 domain has a compact and stable globular structure containing α-helix and β-sheet. GPIbα has a cylindrical and curved structure containing almost only β-sheet, which is loose and flexible. Therefore, GPIbα has larger conformational transition than VWF A1 domain, which is consistent with the RMSD values (Fig. 1c). However, the binding state between VWF A1 domain and GPIbα is always maintained without dissociation during the simulation.

3.2. Binding dynamics in water and physiological saline

As described in Section 2.1, the models of separated VWF A1 domain and GPIbα are constructed. Then the binding process of two proteins is examined by 20 ns MD simulations in both water (simulation trajectory of Sep_0) and physiological saline (simulation trajectory of Sep_0.9).

As shown in Fig. 1a, in water, the minimum distance between two proteins decreases quickly and then reaches a plateau. Similar changes are observed in the distance between the centers of mass. In physiological saline, the minimum distance decreases with obvious fluctuations before 5.0 ns, and then reaches a minimum value. The distance between the centers of mass shows significant fluctuations first, and then turns to decrease after 7.3 ns. These results indicate fast binding in water and slow binding in physiological saline. As shown in Fig. 1b, in water, both the Coulomb and LJ potential energies between VWF A1 domain and GPIbα decrease quickly. However, in physiological saline, the potential energies show little changes before 8.3 ns, and then begin to decrease obviously. Therefore, based on two trajectories of the association process and the slower binding in physiological saline, it is proposed that the

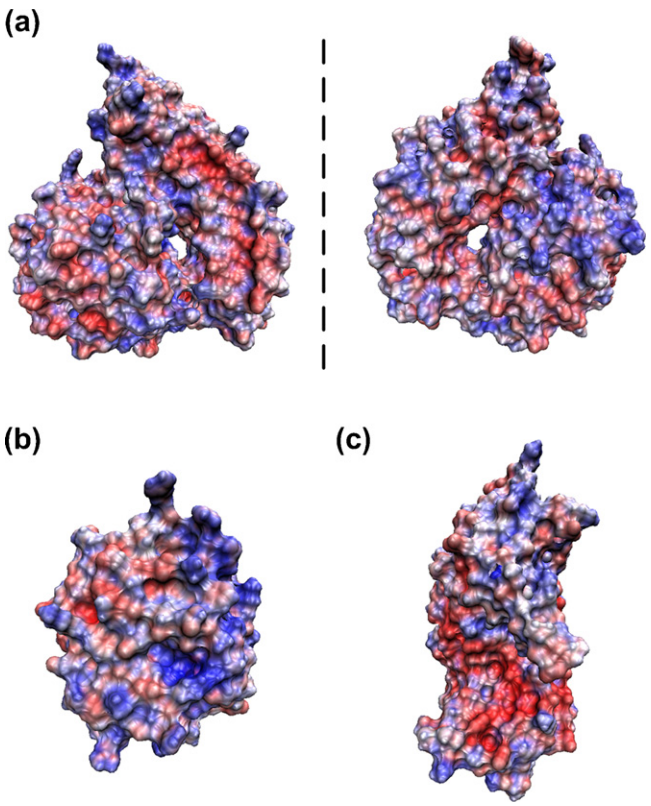

Fig. 4. The electrostatic surface potentials of the proteins. (a) VWF A1–GPIbα complex. (b) VWF A1 domain. (c) GPIbα. The surface is marked in blue and red for positive and negative charge potentials, respectively. The APBS electrostatics analyses are performed using VMD.

long-range electrostatic interactions are dominant to promote the binding between VWF A1 domain and GPIbα. That is, in physiological saline, the blocked electrostatic interactions cause slower binding process.

The secondary structure evolution of the proteins during the binding process is examined by DSSP, as shown in Fig. 2b and c. No significant change of secondary structure is observed during the binding. Furthermore, typical snapshots in each binding process are provided in Fig. 3b and c. Faster binding is observed in water than that in physiological saline, which is consistent with

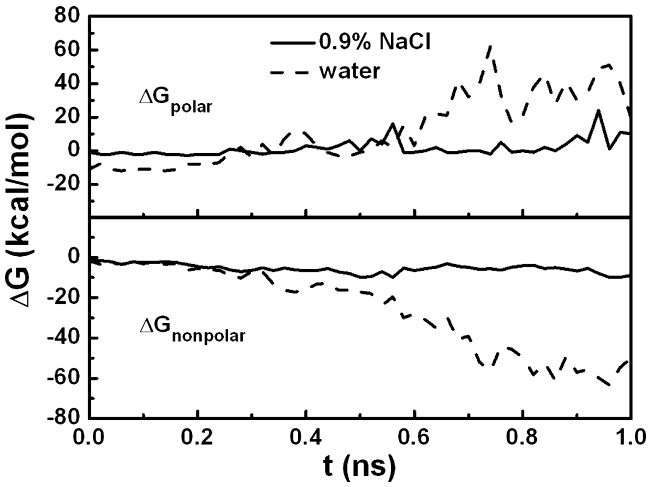

Fig. 5. Free energy decomposition for the initial binding. 51 conformations extracted from the simulation trajectories of Sep_0 or Sep_0.9 from 0 to 1 ns at the interval of 20 ps are used.

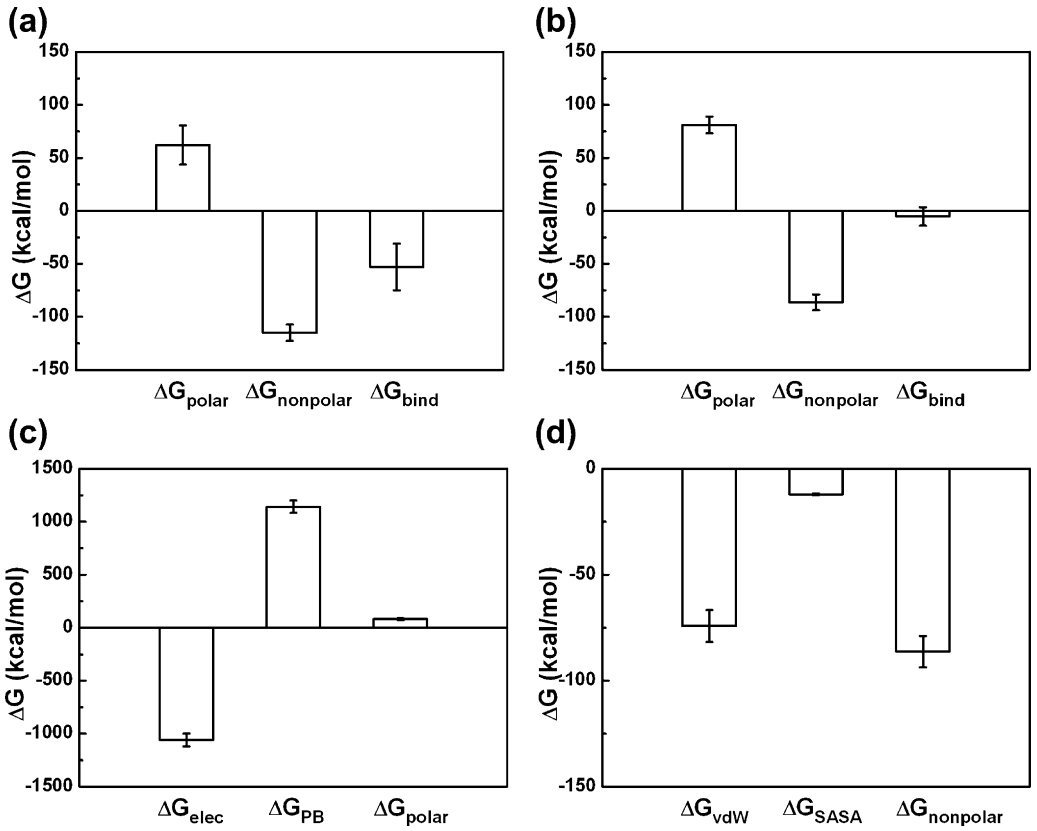

Fig. 6. Free energy decomposition for the binding in water and physiological saline. (a) 11 conformations extracted from the simulation trajectory of Sep_0 from 19 to 20 ns at the interval of 100 ps are used. (b–d) 11 conformations extracted from the simulation trajectory of Sep_0.9 from 19 to 20 ns at the interval of 100 ps are used. The error bars indicate the standard deviations of the 11 conformations.

the results in Fig. 1. The final structure after binding in water is close to its crystal structure from Protein Data Bank. The RMSD is 1.2 nm, which is relatively small considering the large molecular size of the complex. However, larger difference is observed in physiological saline. Because of its globular structure, VWF A1 domain is compact and stable, leading to little conformational transition during the binding. This is consistent with the small R_g and RMSD values (Fig. 1c). However, as GPIbα is an elongated and curved protein containing almost only β-sheet, its loose and flexible structure causes more conformational transition during the binding. This is consistent with the large R_g and RMSD values (Fig. 1c).

For examination of the salt bridges in the complex, the APBS electrostatics analysis is performed to show the electrostatic surface potentials of VWF A1 domain, GPIbα, and their complex, as shown in Fig. 4. Patches of opposite charges are observed at the interface between VWF A1 domain and GPIbα (Fig. 4a). Moreover, as shown in Fig. 4b and c, at the complementary regions of two proteins, major positive charge potentials are observed at the surface of VWF A1 domain, while major negative charge potentials are observed at that of GPIbα.

3.3. Free energy decomposition

The MM–PBSA approach is used to identify the important interactions between VWF A1 domain and GPIbα. The initial stage of binding is analyzed, as shown in Fig. 5. Herein, 51 conformations are extracted from the simulation trajectories of Sep_0 or Sep_0.9 from 0 to 1 ns at the interval of 20 ps. In water (dash lines in Fig. 5, conformations from Sep_0), from 0 to 0.18 ns, negative ΔG_{polar} is always observed, with larger magnitude than $\Delta G_{nonpolar}$. The total binding free energy ΔG_{bind} (the sum of ΔG_{polar} and $\Delta G_{nonpolar}$, Eq. 9) is negative, mainly contributed by ΔG_{polar}. For example, for the conformation at 0 ns in Sep_0, 87% of ΔG_{bind} is contributed by ΔG_{polar} ($\Delta G_{polar} = -11$ kcal/mol, $\Delta G_{nonpolar} = -1.7$ kcal/mol, Fig. 5). This result indicates that the electrostatic interactions are dominant for the binding when VWF A1 domain and GPIbα are far from each other (d_{min} larger than 0.6 nm and d_{com} larger than 4.1 nm, Fig. 1a). Thereafter, increased ΔG_{polar} and decreased $\Delta G_{nonpolar}$ are observed with decreased distance between two proteins (Fig. 1a and Fig. 5). From 0.6 ns, ΔG_{polar} becomes positive, while $\Delta G_{nonpolar}$ becomes more negative, leading to negative ΔG_{bind}. This result indicates that the binding between close VWF A1 domain and GPIbα is maintained by the hydrophobic interactions rather than the electrostatic interactions. For conformations in physiological saline (solid lines in Fig. 5, conformations from Sep_0.9), similar results are observed. However, the blocked electrostatic interactions in physiological saline cause slower binding process, and thus the magnitudes of ΔG_{polar}, $\Delta G_{nonpolar}$, and ΔG_{bind} are much smaller than those in water. Therefore, it is proposed that the long-range electrostatic interactions promote the initial binding between VWF A1 domain and GPIbα. However, hydrophobic interactions are responsible for maintaining the complex formation when the two proteins are close to each other.

In addition, the free energy decomposition results are presented in Fig. 6 to explore the important interactions type for complex formation, using 11 conformations from the simulation trajectories of Sep_0 or Sep_0.9 from 19 to 20 ns at the interval of 100 ps. The negative ΔG_{bind} as a sum of positive ΔG_{polar} and negative $\Delta G_{nonpolar}$ is observed, as shown in Fig. 6a and b, indicating favorable complex formation. It should be noted that the negative ΔG_{elec} is diminished by the positive ΔG_{PB} (Fig. 6c). That is, the favorable electrostatic interactions between proteins are used to compensate the unfavorable solvation effect. Meanwhile, as shown in Fig. 6d, the negative $\Delta G_{nonpolar}$ is contributed by negative ΔG_{vdW} (−74 kcal/mol) and

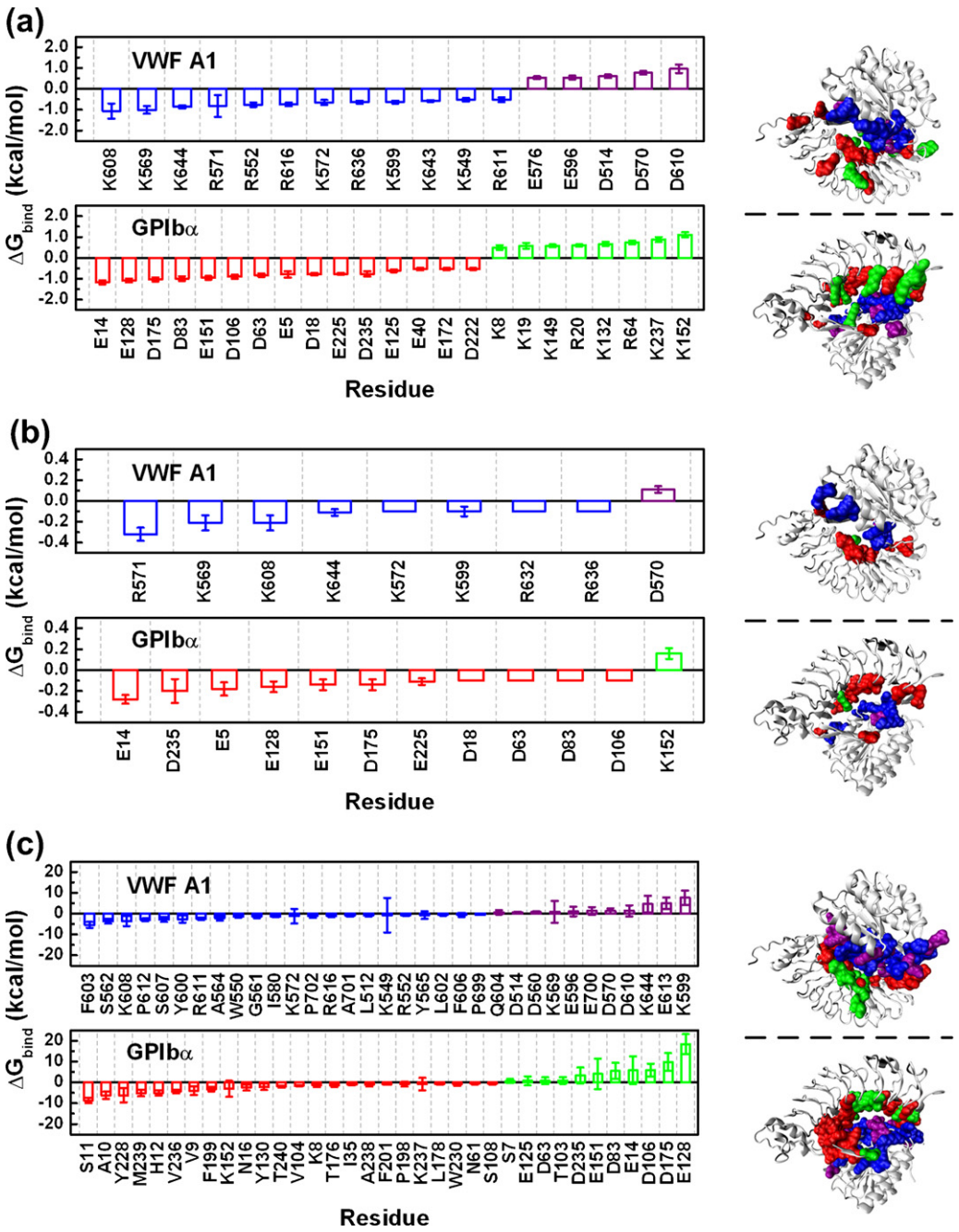

Fig. 7. Binding free energy contribution of each residue in VWF A1 domain and GPIbα. (a) Residues making significant contributions for the initial binding in water. (b) Residues making significant contributions for the initial binding in physiological saline. (c) Residues making significant contributions for the final complex formation. 10 conformations extracted from the simulation trajectories of Sep_0 and Sep_0.9 from 0 to 0.18 ns at the interval of 20 ps are used for (a) and (b), respectively. 11 conformations extracted from Com_0.9 from 19 to 20 ns at the interval of 100 ps are used for (c). Residues making $|\Delta G_{bind}| \geq 0.5$ kcal/mol for (a) and (c), and $|\Delta G_{bind}| \geq 0.1$ kcal/mol for (b) are labeled. The error bars indicate the standard deviations.

negative ΔG_{SASA} (−12 kcal/mol). The negative ΔG_{SASA} is consistent with the loss of SASA as the two proteins associate. The negative ΔG_{vdW} and negative ΔG_{SASA} suggest that both the protein-protein vdW interactions and the nonpolar desolvation upon binding are favorable for complex formation. That is, the favorable hydrophobic contributions are enhanced by the favorable solvation effect. Therefore, from these conformations of the complex, it can be seen that the solvation effect is favorable for hydrophobic interactions while unfavorable for electrostatic interactions. So, the complex formation is maintained by the hydrophobic interactions rather than the electrostatic interactions.

3.4. Identification of hot spots

Several experimental studies on binding sites have been reported. Matsushita et al. [13] reported that K599 interacts directly with GPIbα. Uff et al. [22] thought that E14, D18, E40, D63, D83, D106, E128, E151, and D175 are possible binding surface for interaction with VWF A1. Peng et al. [51] reported that the mutations E128A and D175A almost completely abolished ristocetin-induced VWF binding, and failed to adhere to the VWF surface. Shimizu et al. [52] reported that E128 and D175 are the binding sites for VWF. Therefore, based on the simulation results, the residues

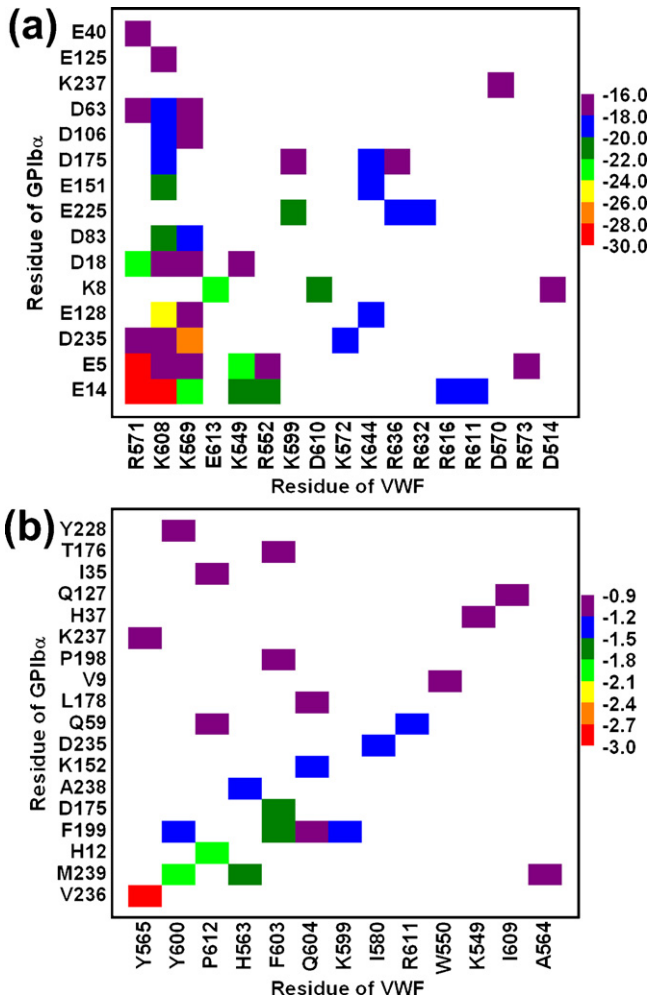

Fig. 8. Pair interaction energy analysis between VWF A1 domain and GPIbα: (a) electrostatic interaction potential energy in the initial binding; (b) vdW interaction potential energy in the final complex formation. Panels are colored according to the interaction energy (in kcal/mol) of each residue pair. Interaction energy ranges from red (most negative) to purple (most positive). Only the residues with significant interaction are displayed.

having large free energy contributions for promoting the initial binding and complex formation are identified, as shown in Fig. 7. The criterion of ±0.5 kcal/mol and ±0.1 kcal/mol are employed for the conformations in water and physiological saline, respectively. Smaller value of criterion is used in physiological saline due to the smaller energy values than that in water (Fig. 5).

As shown in Fig. 7a and b (10 conformations from the simulation trajectories of Sep_0 or Sep_0.9 from 0 to 0.18 ns at the interval of 20 ps), in GPIbα, the most important residues favorable for binding are all negatively charged E or D. These residues are attractive to the VWF A1 domain, and thus are favorable for binding in both water and physiological saline. For example, the residues E14, E128, D175, D83, E151, D106, D63, E5, D18, E225, D235 in GPIbα, and K608, K569, K644, R571, K572, R636, K599 in VWF A1 domain are the residues making large contributions for binding in water, with $\Delta G_{bind} \leq -0.5$ kcal/mol. Within these residues, the electrostatic interaction pairs with significant electrostatic interaction potential energies are shown in Fig. 8a. In physiological saline, these residues are also the most important residues favorable for binding, with $\Delta G_{bind} \leq -0.1$ kcal/mol. So, these residues are identified as the hot spots making dominant favorable contributions for the initial binding between VWF A1 domain and GPIbα, which is consistent with the experimental results as mentioned above. Residues such as E125, E40 in GPIbα, and R552, R616, K643, K549 in VWF A1 domain make contributions for binding in water (with $\Delta G_{bind} \leq -0.5$ kcal/mol) and in physiological saline (with $\Delta G_{bind} > -0.1$ kcal/mol), residue R632 in VWF A1 domain makes contribution for binding in physiological saline (with $\Delta G_{bind} \leq -0.1$ kcal/mol) and in water (with $\Delta G_{bind} > -0.5$ kcal/mol). The free energy decomposition can be used to evaluate the relative importance of individual residue. And the contribution of individual residue for binding is dependent on the solution condition. In the present study, the hot spots are identified considering the solution condition. Therefore, these residues are not considered as the most important ones for binding. Then from the simulation results, it can be seen that all the most important residues for binding are charged residues, including negatively charged E and D in GPIbα, and positively charged K and R in VWF A1 domain. On the contrary, positively charged K and R in GPIbα, are repulsive to the VWF A1 domain, while negatively charged E and D in VWF A1 domain, are repulsive to the GPIbα. These residues are unfavorable for binding. However, the unfavorable contributions are less than the favorable contributions, leading to successful binding. Therefore, it can be seen from the simulations that the electrostatic interactions are dominant to promote the initial binding, providing further details for the results in Fig. 5.

Moreover, the most important residues for the formation of the final complex ($d_{com} < 3.5$ nm) are identified, using 11 conformations from the simulation trajectory of Com_0.9 from 19 to 20 ns at the interval of 100 ps. As shown in Fig. 7c, the hot spots for complex formation are different from the ones for promoting the initial binding. Major favorable contributions for complex formation are hydrophobic contributions (72%) made by residues with a wide distribution at the binding interface. Residues S11, A10, Y228, M239, H12, V236, V9, F199, K152 in GPIbα, and residues F603, S562, K608, P612, S607, Y600 in VWF A1 domain make the largest favorable contributions, with $\Delta G_{bind} \leq -2.5$ kcal/mol. Within these residues, F199 ($\Delta G_{nonpolar} = -4.03$ kcal/mol), F603 ($\Delta G_{nonpolar} = -3.97$ kcal/mol), Y600 ($\Delta G_{nonpolar} = -3.95$ kcal/mol) and M239 ($\Delta G_{nonpolar} = -3.84$ kcal/mol) are located at the binding interface and make the largest favorable hydrophobic contributions. In addition, pairs Y600 and M239, F199 and F603, F199 and Y600 have the strongest vdW interactions (indicated by lowest potential energies in Fig. 8b). As reported by Huizinga et al. [21], interaction between V239 and Y600 in the mutation M239V is significant for platelet-type von Willebrand disease. Herein, the simulation results suggest that the M239 is an important binding site with significant hydrophobic contribution favorable for the final complex formation.

However, the residues making significant unfavorable contributions are almost all charged residues. For example, residues D235, E151, D83, E14, D106, D175, E128 in GPIbα, and residues K644, E613, K599 in VWF A1 domain make the largest unfavorable contributions, with $\Delta G_{bind} > 2.5$ kcal/mol. So, the total electrostatic interactions are unfavorable for complex formation. Therefore, it can be seen from the simulations that the complex formation is maintained by hydrophobic interactions. In comparison with the initial binding, some charged residues unfavorable for the initial binding change to favorable for complex formation, such as K152 in GPIbα with positive ΔG_{bind} in Fig. 7a and b, and negative ΔG_{bind} in Fig. 7c. However, more charged residues favorable for the initial binding change to unfavorable for complex formation, such as D235, E151, D83, E14, D106, D175, E128 in GPIbα, and K644, K599 in VWF A1 domain. Combined with Fig. 6, it can be seen that the favorable electrostatic interactions are canceled by the solvation effect, and turn to be unfavorable for complex formation.

Protein–protein association has been well examined using Brownian dynamics (BD) simulations, where the protein molecules, modeled as rigid bodies are simulated in a continuum solvent for

10 us [53–55]. MD simulation has also been performed to examine the conformational transitions such as the refolding of a protein dimer in explicit water [56]. In the present study, MM–PBSA approach is utilized to identify hot spots for protein-protein association based on all-atom MD simulations. The present study highlights the importance to understand the natures of electrostatic and hydrophobic interactions. Our results suggest that the different natures of electrostatic and hydrophobic interactions are responsible for their different roles in the complex formation. The electrostatic interaction is a kind of long-range interaction, while the hydrophobic interaction is not. Therefore, the electrostatic interaction is able to provide driving forces when separated proteins are far from each other, while the hydrophobic interaction can only be dominant when proteins are close. Also, it can be seen that molecular dynamics simulations are useful to investigate the microscopic process. However, if we only focus on the results from the dynamics simulations in the present study, the important role of the hydrophobic interactions may be neglected. For MM–PBSA analysis, if the extracted conformations are all stable complexes, the results will focus on that the hydrophobic interactions contribute to the complex formation. In this case, the role of electrostatic interactions to promote the initial binding may be neglected. It can be seen that the computational approach is a good way to analyze the binding free energy of the complex in a thermodynamic sense [57–61]. However, to avoid missing important details, we suggest that it should be considered more carefully on how to utilize the MM–PBSA technique. Overall, for full appreciation of the binding it is necessary to investigate not only in a kinetic sense, but also in a thermodynamic sense.

4. Conclusions

In the present study, molecular basis of the initial platelet adhesion in arterial thrombosis has been investigated based on two simulations of the association process. Although only two simulations (20 ns each) of the association process have been performed due to both the large simulation system and the limited computational resources, comprehensive analysis of the simulations has provided a convergent description about the association, which is consistent with macroscopic experimental results. The results indicate that the electrostatic interactions provide long-range driving forces to promote the initial binding between VWF A1 domain and GPIbα, and subsequently the hydrophobic interactions are dominant to maintain the complex formation. Moreover, the hot spots for binding have been identified, including E14, E128, D175, D83, E151, D106, D63, E5, D18, E225, D235 in GPIbα, and K608, K569, K644, R571, K572, R636, K599 in VWF A1 domain. The hot spots for complex formation include F199, M239, F603 and Y600. These hot spots are primary targets to inhibit the VWF A1-GPIbα binding. Therefore, this work has provided valuable molecular insights into the VWF A1-GPIbα interactions. It would be beneficial to understand the molecular mechanisms of arterial thrombosis and the studies are crucial for accelerating the development of novel and more potent antithrombotic agents.

Acknowledgments

This work was supported by the Natural Science Foundation of China (Nos. 20636040, 20976126 and 21006069) and the Innovation Foundation of Tianjin University.

References

[1] B. Furie, B.C. Furie, Mechanisms of disease: mechanisms of thrombus formation, New England Journal of Medicine 359 (2008) 938–949.
[2] T.A. Meadows, D.L. Bhatt, Clinical aspects of platelet inhibitors and thrombus formation, Circulation Research 100 (2007) 1261–1275.
[3] A.D. Blann, Platelets The universal killer, Biochimica et Biophysica Acta-Molecular Basis of Disease 1772 (2007) 715–717.
[4] R.K. Andrews, E.E. Gardiner, Y. Shen, M.C. Berndt, Platelet interactions in thrombosis, IUBMB Life 56 (2004) 13–18.
[5] R.A. Ajjan, R. Ariens, Cardiovascular disease and heritability of the prothrombotic state, Blood Reviews 23 (2009) 67–78.
[6] B.J. Fredrickson, J.F. Dong, L.V. McIntire, J.A. Lopez, Shear-dependent rolling on von Willebrand factor of mammalian cells expressing the platelet glycoprotein Ib-IX–V complex, Blood 92 (1998) 3684–3693.
[7] R. Romijn, B. Bouma, W. Wuyster, P. Gros, J. Kroon, J.J. Sixma, E.G. Huizinga, Identification of the collagen-binding site of the von Willebrand factor A3-domain, Journal of Biological Chemistry 276 (2001) 9985–9991.
[8] M. Gawaz, Role of platelets in coronary thrombosis and reperfusion of ischemic myocardium, Cardiovascular Research 61 (2004) 498–511.
[9] P. Siljander, I. Munnix, P.A. Smethurst, H. Deckmyn, T. Lindhout, W.H. Ouwehand, R.W. Farndale, J. Heemskerk, Platelet receptor interplay regulates collagen-induced thrombus formation in flowing human blood, Blood 103 (2004) 1333–1341.
[10] Z.M. Ruggeri, J.A. Dent, E. Saldivar, Contribution of distinct adhesive interactions to platelet aggregation in flowing blood, Blood 94 (1999) 172–178.
[11] D. Varga-Szabo, I. Pleines, B. Nieswandt, Cell adhesion mechanisms in platelets, Arteriosclerosis Thrombosis and Vascular Biology 28 (2008) 403–412.
[12] J. Emsley, M. Cruz, R. Handin, R. Liddington, Crystal structure of the von Willebrand factor A1 domain and implications for the binding of platelet glycoprotein Ib, Journal of Biological Chemistry 273 (1998) 10396–10401.
[13] T. Matsushita, D. Meyer, J.E. Sadler, Localization of von Willebrand factor-binding sites for platelet glycoprotein Ib and botrocetin by charged-to-alanine scanning mutagenesis, Journal of Biological Chemistry 275 (2000) 11044–11049.
[14] M.A. Cruz, T.G. Diacovo, J. Emsley, R. Liddington, R.I. Handin, Mapping the glycoprotein Ib-binding site in the von Willebrand factor A1 domain, Journal of Biological Chemistry 275 (2000) 19098–19105.
[15] J. Rivera, M.L. Lozano, L. Navarro-Nunez, V. Vicente, Platelet receptors and signaling in the dynamics of thrombus formation, Hematologica – The Hematology Journal 94 (2009) 700–711.
[16] N.A. Mody, O. Lomakin, T.A. Doggett, T.G. Diacovo, M.R. King, Mechanics of transient platelet adhesion to von Willebrand factor under flow, Biophysical Journal 88 (2005) 1432–1443.
[17] J.M. Gibbins, Platelet adhesion signalling and the regulation of thrombus formation, Journal of Cell Science 117 (2004) 3415–3425.
[18] S.P. Jackson, The growing complexity of platelet aggregation, Blood 109 (2007) 5087–5095.
[19] R.K. Andrews, M.C. Berndt, Platelet adhesion: a game of catch and release, Journal of Clinical Investigation 118 (2008) 3009–3011.
[20] B. Savage, F. Almus-Jacobs, Z.M. Ruggeri, Specific synergy of multiple substrate–receptor interactions in platelet thrombus formation under flow, Cell 94 (1998) 657–666.
[21] E.G. Huizinga, S. Tsuji, R. Romijn, M.E. Schiphorst, P.G. De Groot, J.J. Sixma, P. Gros, Structures of glycoprotein Ib alpha and its complex with von Willebrand factor A1 domain, Science 297 (2002) 1176–1179.
[22] S. Uff, J.M. Clemetson, T. Harrison, K.J. Clemetson, J. Emsley, Crystal structure of the platelet glycoprotein Ib alpha N-terminal domain reveals an unmasking mechanism for receptor activation, Journal of Biological Chemistry 277 (2002) 35657–35663.
[23] R.K. Andrews, J.A. Lopez, M.C. Berndt, Molecular mechanisms of platelet adhesion and activation, The International Journal of Biochemistry and Cell Biology 29 (1997) 91–105.
[24] G. Stoll, C. Kleinschnitz, B. Nieswandt, Molecular mechanisms of thrombus formation in ischemic stroke: novel insights and targets for treatment, Blood 112 (2008) 3555–3562.
[25] U. Sachs, B. Nieswandt, In vivo thrombus formation in murine models, Circulation Research 100 (2007) 979–991.
[26] S. Moog, P. Mangin, N. Lenain, C. Strassel, C. Ravanat, S. Schuhler, M. Freund, M. Santer, M. Kahn, B. Nieswandt, C. Gachet, J.P. Cazenave, F. Lanza, Platelet glycoprotein V binds to collagen and participates in platelet adhesion and aggregation, Blood 98 (2001) 1038–1046.
[27] B. Savage, E. Saldivar, Z.M. Ruggeri, Initiation of platelet adhesion by arrest onto fibrinogen or translocation on von Willebrand factor, Cell 84 (1996) 289–297.
[28] M.J. Maxwell, E. Westein, W.S. Nesbitt, S. Giuliano, S.M. Dopheide, S.P. Jackson, Identification of a 2-stage platelet aggregation process mediating shear-dependent thrombus formation, Blood 109 (2007) 566–576.
[29] Y. Shen, G.M. Romo, J.F. Dong, A. Schade, L.V. McIntire, D. Kenny, J.C. Whisstock, M.C. Berndt, J.A. Lopez, R.K. Andrews, Requirement of leucine-rich repeats of glycoprotein (GP) Ib alpha for shear-dependent and static binding of von Willebrand factor to the platelet membrane GP Ib-IX–V complex, Blood 95 (2000) 903–910.
[30] J.H. Cho, D.F. Mosher, Impact of fibronectin assembly on platelet thrombus formation in response to type I collagen and von Willebrand factor, Blood 108 (2006) 2229–2236.
[31] S. Kulkarni, S.M. Dopheide, C.L. Yap, C. Ravanat, M. Freund, P. Mangin, K.A. Heel, A. Street, I.S. Harper, F. Lanza, S.P. Jackson, A revised model of platelet aggregation, Journal of Clinical Investigation 105 (2000) 783–791.
[32] M. Karplus, J.A. McCammon, Molecular dynamics simulations of biomolecules, Natural Structural Biology 9 (2002) 646–652.

[33] V. Daggett, Protein folding-simulation, Chemical Reviews 106 (2006) 1898–1916.
[34] J. Zheng, H. Jang, B. Ma, R. Nussinov, Annular structures as intermediates in fibril formation of Alzheimer A beta (17–42), Journal of Physical Chemistry B 112 (2008) 6856–6865.
[35] J. Zheng, X. Yu, J. Wang, J. Yang, Q. Wang, Molecular modeling of two distinct triangular oligomers in amyloid beta-protein, Journal of Physical Chemistry B 114 (2010) 463–470.
[36] J.E. Straub, D. Thirumalai, Principles governing oligomer formation in amyloidogenic peptides, Current Opinion in Structural Biology 20 (2010) 187–195.
[37] N.G. Sgourakis, M. Merced-Serrano, C. Boutsidis, P. Drineas, Z. Du, C. Wang, A.E. Garcia, Atomic-level characterization of the ensemble of the a beta (1–42) monomer in water using unbiased molecular dynamics simulations and spectral algorithms, Journal of Molecular Biology 405 (2011) 570–583.
[38] N.V. Buchete, R. Tycko, G. Hummer, Molecular dynamics simulations of Alzheimer's beta-amyloid protofilaments, Journal of Molecular Biology 353 (2005) 804–821.
[39] P.M. de, M.G. de, L. Serrano, G. Colombo, Sequence dependence of amyloid fibril formation: insights from molecular dynamics simulations, Journal of Molecular Biology 349 (2005) 583–596.
[40] T. Takeda, D.K. Klimov, Dissociation of A beta (16–22) amyloid fibrils probed by molecular dynamics, Journal of Molecular Biology 368 (2007) 1202–1213.
[41] B. Tarus, J.E. Straub, D. Thirumalai, Structures and free-energy landscapes of the wild type and mutants of the A beta (21–30) peptide are detennined by an interplay between intrapeptide electrostatic and hydrophobic interactions, Journal of Molecular Biology 379 (2008) 815–829.
[42] J. Gsponer, P. Ferrara, A. Caflisch, Flexibility of the murine prion protein and its Asp178Asn mutant investigated by molecular dynamics simulations, Journal of Molecular Graphics and Modeling 20 (2001) 169–182.
[43] J.J. Dumas, R. Kumar, T. McDonagh, F. Sullivan, M.L. Stahl, W.S. Somers, L. Mosyak, Crystal structure of the wild-type von Willebrand factor A1-glycoprotein Ib alpha complex reveals conformation differences with a complex bearing von Willebrand disease mutations, Journal of Biological Chemistry 279 (2004) 23327–23334.
[44] H.J. Berendsen, D. Vanderspoel, R. Vandrunen, Gromacs – a message-passing parallel molecular – dynamics implementation, Computer Physics Communications 91 (1995) 43–56.
[45] E. Lindahl, B. Hess, S.D. van, GROMACS 3.0: a package for molecular simulation and trajectory analysis, Journal of Molecular Modeling 7 (2001) 306–317.
[46] A.D. Mackerell, Empirical force fields for biological macromolecules: overview and issues, Journal of Computational Chemistry 25 (2004) 1584–1604.
[47] C. Yang, D.N. Lu, Z. Liu, How pegylation enhances the stability and potency of insulin: a molecular dynamics simulation, Biochemistry – U.S. 50 (2011) 2585–2593.
[48] B. Huang, F.F. Liu, X.Y. Dong, Y. Sun, Molecular mechanism of the affinity interactions between protein A and human innmunoglobulin G1 revealed by molecular simulations, Journal of Physical Chemistry B 115 (2011) 4168–4176.
[49] N. Todorova, F.S. Legge, H. Treutlein, I. Yarovsky, Systematic comparison of empirical forcefields for molecular dynamic simulation of insulin, Journal of Physical Chemistry B 112 (2008) 11137–11146.
[50] V. Zoete, M. Meuwly, M. Karplus, Study of the insulin dimerization: binding free energy calculations and per-residue free energy decomposition, Proteins 61 (2005) 79–93.
[51] Y.D. Peng, C.N. Shrimpton, J.F. Dong, J.A. Lopez, Gain of von Willebrand factor-binding function by mutagenesis of a species-conserved residue within the leucine-rich repeat region of platelet glycoprotein Ib alpha, Blood 106 (2005) 1982–1987.
[52] A. Shimizu, T. Matsushita, T. Kondo, Y. Inden, T. Kojima, H. Saito, M. Hirai, Identification of the amino acid residues of the platelet glycoprotein Ib (GPIb) essential for the von Willebrand factor binding by clustered charged-to-alanine scanning mutagenesis, Journal of Biological Chemistry 279 (2004) 16285–16294.
[53] P. Mereghetti, R.R. Gabdoulline, R.C. Wade, Brownian dynamics simulation of protein solutions structural and dynamical properties, Biophysical Journal 99 (2010) 3782–3791.
[54] A. Spaar, C. Dammer, R.R. Gabdoulline, R.C. Wade, V. Helms, Diffusional encounter of barnase and barstar, Biophysical Journal 90 (2006) 1913–1924.
[55] R.R. Gabdoulline, R.C. Wade, Protein–protein association: investigation of factors influencing association rates by Brownian dynamics simulations, Journal of Molecular Biology 306 (2001) 1139–1155.
[56] L.T. Chong, C.D. Snow, Y.M. Rhee, V.S. Pande, Dimerization of the p53 oligomerization domain: identification of a folding nucleus by molecular dynamics simulations, Journal of Molecular Biology 345 (2005) 869–878.
[57] H. Zou, C. Luo, S. Zheng, X. Luo, W. Zhu, K. Chen, J. Shen, H. Jiang, Molecular insight into the interaction between IFABP and PA by using MM–PBSA and alanine scanning methods, Journal of Physical Chemistry B 111 (2007) 9104–9113.
[58] J. Zeng, W. Li, Y. Zhao, G. Liu, Y. Tang, H. Jiang, Insights into ligand selectivity in estrogen receptor isoforms: molecular dynamics simulations and binding free energy calculations, Journal of Physical Chemistry B 112 (2008) 2719–2726.
[59] H. Gohlke, C. Kiel, D.A. Case, Insights into protein–protein binding by binding free energy calculation and free energy decomposition for the Ras–Raf and Ras–RalGDS complexes, Journal of Molecular Biology 330 (2003) 891–913.
[60] W. Wang, P.A. Kollman, Free energy calculations on dimer stability of the HIV protease using molecular dynamics and a continuum solvent model, Journal of Molecular Biology 303 (2000) 567–582.
[61] V. Tsui, D.A. Case, Calculations of the absolute free energies of binding between RNA and metal ions using molecular dynamics simulations and continuum electrostatics, Journal of Physical Chemistry B 105 (2001) 11314–11325.